Optical, thermo-optic, electro-optic, and photoelastic properties of bismuth germanate ($Bi_4Ge_3O_{12}$)

P. A. Williams, A. H. Rose, K. S. Lee, D. C. Conrad, G. W. Day, and P. D. Hale

To assess the suitability of bismuth germanate as an electro-optic material for high precision applications, we have confirmed and extended previous data on its refractive index, electro-optic tensor element r_{41}, and thermal expansion coefficient. In addition, we have measured the thermo-optic coefficient dn/dT, the temperature dependence of the electro-optic coefficient, and the stress-optic tensor elements. From the stress-optic tensor elements and previously published data, we have computed the strain-optic tensor elements. The index of refraction is given, to a good approximation, by the single-term Sellmeier equation, $n^2 - 1 = s_0\lambda_0^2/[1 - (\lambda_0/\lambda)^2]$, with $s_0 = 95.608\ \mu m^{-2}$ and $\lambda_0 = 0.1807$ μm. The thermo-optic coefficient is $3.9 \times 10^{-5}/°C$ at 632.8 nm and $3.5 \times 10^{-5}/°C$ at 1152.3 nm. The electro-optic tensor element varies between approximately 1.05 and 1.11 pm/V over the spectral range of 550–1000 nm; its normalized effective change with temperature is approximately $1.54 \times 10^{-4}/°C$. The thermal expansion coefficient is $6.3 \times 10^{-6}/°C$ over the range 15–125 °C. Values of the stress-optic tensor elements are $q_{11} - q_{12} = -2.995 \times 10^{-13}\ m^2/N$ and $q_{44} = -0.1365 \times 10^{-12}\ m^2/N$. The strain-optic tensor elements are $p_{11} - p_{12} = -0.0266$ and $p_{44} = -0.0595$.

Key words: Bismuth germanate, electro-optic, refractive index, strain optic, stress optic, temperature dependence, thermal expansion.

1. Introduction

Bismuth germanate ($Bi_4Ge_3O_{12}$, or BGO) is an attractive material for those applications of the electro-optic effect, such as voltage and electric field sensors, in which precision (reproducibility or stability) is more important than sensitivity.[1] It is a cubic crystal of point group symmetry $43m$ and does not exhibit natural linear birefringence, which is a major cause of instability in many electro-optic devices. Neither does BGO exhibit circular birefringence (optical activity), which quenches the electro-optic effect and reduces its stability. BGO is transparent from approximately 350 nm to 4 μm, which suggests that its optical properties in the 800–1500-nm spectral region (where most sensors operate) should be relatively stable with temperature. BGO is free from pyroelectric effects and is available in large crystals with good optical quality.

To assess the potential of BGO as an electro-optic material more thoroughly, we have undertaken a study of its relevant optical properties. Measurements of refractive index n and electro-optic tensor element r_{41} have been reported by Nitsche,[2] Bortfeld and Meier,[3] Montemezzani *et al.*,[4] and Kamada and Kakishita.[5] A measurement of the thermal expansion coefficient was reported by Schweppe.[6] We have confirmed and extended their data and have, in addition, determined temperature derivatives dn/dT and $d(n_0^3 r_{41})/dT$ over a range of wavelengths. We have also determined the stress-optic tensor elements at one wavelength and, using previously reported elastic constants,[6] computed the strain-optic tensor elements.

2. Optical Properties

A. Index of Refraction Measurements

To obtain the index of refraction, we used a prism spectroscope to measure the angle of minimum deviation of an unoriented prism. This yields the index of refraction relative to air. The experimental

When this research was performed, the authors were with the Optoelectronics Division, National Institute of Standards and Technology, 815, Boulder, Colorado 80303. K. S. Lee is now with the Department of Electronic Engineering, Sung Kyun Kwan University, 300 Chunchun-Dong, Suwon, South Korea 440-746. D. C. Conrad is now with Seiko Instruments, 2990 West Lomita Boulevard, Torrence, California 90505.

Received 5 October 1995; revised manuscript received 18 December 1995.

0003-6935/96/193562-08$10.00/0

arrangement and technique were similar to that shown and described in Ref. 7. We used a tungsten–halogen lamp with narrow-band interference filters as the source and an infrared viewer for detection. The prism has an apex angle, β, of $34.27 \pm 0.01°$. Our divided circle spectrometer has a resolution of $0.5'$, which we take as our estimate of the uncertainty in the angle of deviation. The expression for the index of refraction as a function of the apex angle and the angle of minimum deviation, θ_m, is

$$n = \frac{\sin(\theta_m/2 + \beta/2)}{\sin(\beta/2)}. \tag{1}$$

The uncertainties in n resulting from uncertainties in β and θ_m are given by[8]

$$\Delta n_\beta = \frac{n}{2}\left[\cot\left(\frac{\beta}{2}\right) - \cot\left(\frac{\beta + \theta_m}{2}\right)\right]\Delta\beta, \tag{2}$$

$$\Delta n_{\theta_m} = \frac{n}{2}\cot\left(\frac{\beta + \theta_m}{2}\right)\Delta\theta_m. \tag{3}$$

Using these expressions we obtain $\Delta n_\beta = \pm 0.0003$ and $\Delta n_{\theta_m} = \pm 0.0002$. We choose the sum of the magnitudes of these as an estimate of the total uncertainty in the measurement ($\Delta n = \pm 0.0005$).

For the prisms used, θ_m is approximately 40°. Our determinations of the index of refraction at various wavelengths are listed in Table 1 along with previous measurements.[3,4] Our data, the previous data, and the combined set were each fitted to a single-term Sellmeier equation of the form

$$n^2 - 1 = \frac{s_0\lambda_0{}^2}{1 - (\lambda_0/\lambda)^2}. \tag{4}$$

The values of s_0 and λ_0 from a least-squares fit for each case are listed in Table 2. Figure 1 shows all of the index of refraction data along with the best-fit curve for the complete data set.

Table 1. Measured Index of Refraction for Bismuth Germanate

	Index of Refraction		
Wavelength (nm)	This Study (±0.0005)	Ref. 3 (±0.0003)	Ref. 4
305.4			2.410 ± 0.003
334.5			2.326 ± 0.003
351.1			2.291 ± 0.003
363.9			2.268 ± 0.003
407.7		2.2152	
435.8		2.1836	
457.9			2.167 ± 0.001
467.8		2.1597	
480		2.1522	
488.9			2.148 ± 0.001
508		2.1373	
514			2.135 ± 0.001
546.1		2.1218	
550	2.1204		
577		2.1116	
589.3		2.1081	
600	2.1058		
632.8		2.0975	2.097 ± 0.001
633	2.0972		
643		2.0952	
750	2.0786		
800	2.0723		
850	2.0678		
900	2.0635		
950	2.0601		
1000	2.0578		

B. dn/dT and α Measurements

To measure the temperature derivative of index of refraction dn/dT, sometimes called the thermo-optic coefficient, we used the method of Fizeau interference fringes described by Feldman *et al.*[9] An unoriented specimen with two polished parallel faces is placed in the collimated beam of a high-coherence laser. Interference fringes in the light reflected from the two surfaces shift with temperature as the optical path length changes. The shifts are monitored with a detector that is small compared with the fringe spacing. In terms of fringe count M, the change in the index of refraction between two temperatures T_1 and T_2 is given by

$$|n_2 - n_1| = \frac{M\lambda}{2h_1} - n_1\frac{\Delta h}{h_1}, \tag{5}$$

where λ is the vacuum wavelength, h_1 is the physical thickness at temperature T_1, Δh is the change in thickness, and a term of the form $1 + \Delta h/h_1$ in the denominator has been neglected. If the linear thermal expansion properties of the material are known, we can thereby obtain $\Delta n/\Delta T$ over the range of measurement. In particular, if thermal expansion coefficient α of the material is effectively constant, we can rewrite Eq. (5) as

$$\frac{\Delta n}{\Delta T} = \frac{M\lambda}{2h_1\Delta T} - n_1\alpha. \tag{6}$$

We can measure thermal expansion by placing wedged optical flats, larger than the specimen, in contact with its two polished surfaces and monitoring the fringe shifts resulting from interference between the surfaces of the flats, to one side of the specimen.[9] In practice, most of the polished surfaces of the specimen are etched away, leaving three pads, upon which the flats rest more securely. If the measurements are performed in air, the change in h between temperatures T_2 and T_1 is given, as a

Table 2. Parameters of the Sellmeier Equation for BGO

Parameter	This Study	Ref. 3	Combined
s_0 (μm^{-2})	99.250	95.080	95.608
λ_0 (μm)	0.1776	0.1811	0.1807

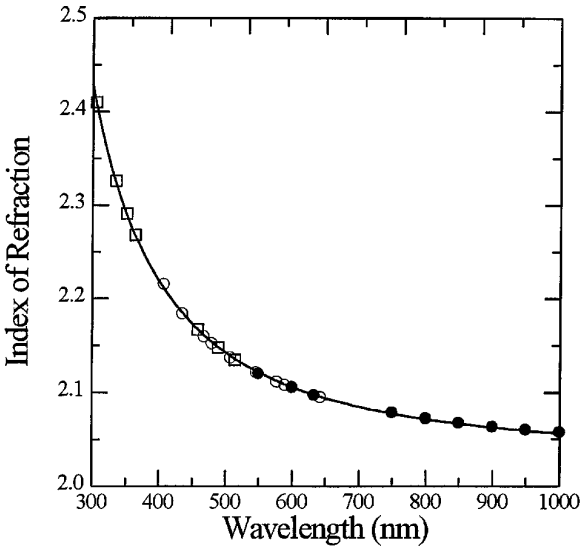

Fig. 1. Index of refraction data for BGO. The open circles are from Ref. 3 and the squares are from Ref. 4. The solid circles are from this study. The curve is Eq. (4), with the parameters taken from the combined set of data in Table 2.

function of the fringe shift, by

$$\Delta h \equiv h_2 - h_1 = \frac{M\lambda}{2n_{a2}} - h_1 \frac{\Delta n_a}{n_{a2}}, \tag{7}$$

where $\Delta n_a = n_{a2} - n_{a1}$ is the difference in index of refraction of air between temperatures T_2 and T_1. The thermal expansion coefficient is then

$$\alpha \equiv \frac{\Delta h}{h_1 \Delta T} = \frac{M\lambda}{2h_1 n_{a2} \Delta T} - \frac{\Delta n_a}{n_{a2} \Delta T}, \tag{8}$$

where $\Delta T = T_2 - T_1$.

From the research of Barrell and Sears,[10] we estimated quantity $\Delta n_a/(n_{a\,2}\Delta T)$ to be

$$\frac{\Delta n_a}{n_{a2}\Delta T} \approx (-0.6 \pm 0.06) \times 10^{-6}/^{\circ}\mathrm{C}. \tag{9}$$

This represents an approximately 10% contribution to the value of α obtained from Eq. (8).

An ambiguity of sign remains in both the thermal expansion and thermo-optic measurements. We expected α to be positive and confirmed that mechanically. Then we determined the sign of the change in optical thickness by placing the specimen in a highly divergent beam and observing whether the circular fringes expand or contract with temperature. We observed expanding fringes with increasing temperature, which corresponds to an increase in the optical thickness with temperature.[9,11]

Figure 2 shows a schematic diagram of the experimental apparatus for the measurement of α and dn/dT. Two He–Ne lasers, one at 632.8 nm and one at 1152.3 nm, were used as sources. The specimen rests in a copper oven that is wrapped with a heating

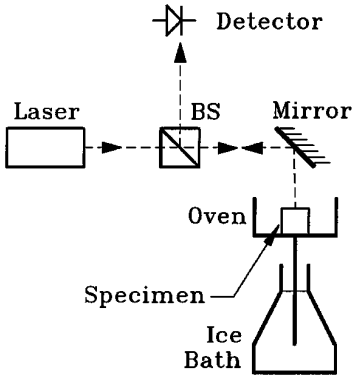

Fig. 2. Apparatus for measuring dn/dT and α; BS, beam splitter.

element. A copper rod extends from the chamber to an ice bath, allowing measurements below room temperature. Two thermocouples, attached to opposite sides of the specimen, provide continuous measurement of the temperature of the specimen and an indication of its uniformity. Over the range of measurements (15–125 °C) the thermocouples agreed to within much less than 1 °C, except at the highest temperatures, where they typically differed by as much as 1 °C.

Values of dn/dT and α were measured over the range 15–125 °C, with individual data points coming from an average over an approximately 10 °C temperature range. The repeatability of the data points at specific temperatures was only ± 5 to $\pm 10\%$; however, the total uncertainties of the average values of α and dn/dT over the full temperature range are closer to $\pm 5\%$. The value of α was $(6.3 \pm 0.3) \times 10^{-6}/^{\circ}\mathrm{C}$, over the full temperature range 15–125 °C. The average values of dn/dT for 632.8 nm and 1152.3 nm over that same range are shown in Table 3. Within the measurement uncertainty, α and dn/dT were independent of temperature.

We are not aware of any previous determinations of dn/dT for BGO. A thermal expansion coefficient measurement of $5 \times 10^{-6}/^{\circ}\mathrm{C}$ has been reported.[6] If the previous result was taken near room temperature, our value is approximately 20% larger.

3. Electro-Optic Properties

The linear electro-optic effect, with which we are concerned here, is described by a third rank tensor, commonly represented as a 6×3 matrix. For crystals with point group symmetry $\bar{4}3m$, the matrix has three equal, nonzero elements, $r_{41} = r_{52} = r_{63}$. Possible configurations for using the electro-optic effect in this crystal class have been described in detail by Namba[12] and Yariv and Yeh.[13] The opti-

Table 3. Thermo-Optic Coefficients of BGO

λ (nm)	dn/dT (°C^{-1})
632.3	$(3.9 \pm 0.2) \times 10^{-5}$
1152.3	$(3.5 \pm 0.2) \times 10^{-5}$

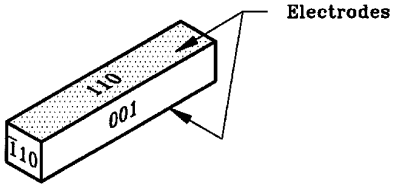

Fig. 3. Orientation of the crystal used in the electro-optic measurements.

mum configuration is for light to propagate in the $(\bar{1}10)$ direction with an electric field applied along the (110) direction (Fig. 3). The axes of induced linear birefringence are along the (111) and $(11\bar{1})$ directions at $\pm 45°$ to the direction of the applied field. The induced phase retardance for this case is

$$\delta_E = \frac{2\pi}{\lambda} n_0^3 r_{41} V \frac{h}{d}, \tag{10}$$

where n_0 is the unperturbed refractive index of the crystal, V is the voltage applied between the (110) faces, h is the length of the crystal along the optical propagation direction, d is the distance between the electrodes, and λ is the vacuum wavelength.

Two experimental setups were assembled to measure $n_0^3 r_{41}$ and $\mathrm{d}(n_0^3 r_{41})/\mathrm{d}Tn_0^3 r_{41}$ separately. Both setups have an input polarizer at $\theta = 0°$, a quarter-wave plate at $\theta = 45°$, the BGO crystal with δ_E between the $\theta = \pm 45°$ axes, a residual stress birefringence δ_S between the 0° and 90° axes caused by cutting and polishing of the crystal, and an output polarizing beam splitter or analyzer at $\theta = 0°$ and $\theta = 90°$. The Appendix presents a derivation of the transmittance (intensity response function), using Jones matrices, for the above assemblies. This transmittance is

$$R(\delta_E, \delta_S)_{\pm} = \Gamma_{\pm}\left(1 \pm \delta_E \frac{\sin 2\phi}{2\phi}\right), \tag{11}$$

where $\pm$ refers to the two positions of the output polarizer, $\Gamma_{\pm}$ is the static transmittance of the optical system, and $2\phi = (\delta_E{}^2 + \delta_S{}^2)^{1/2}$.

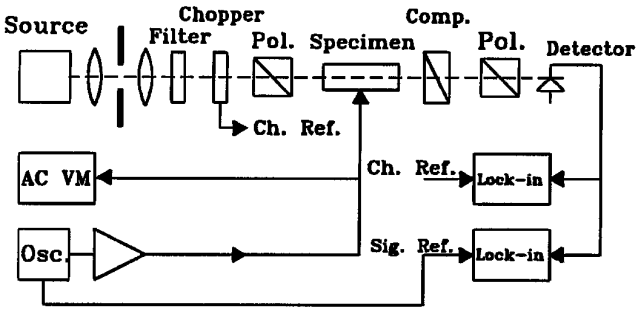

Fig. 4. System for measuring $n_0^3 r_{41}$; AC VM, ac voltmeter.

A. $n_0^3 r_{41}$ and r_{41} Measurements

We determined the quantity $n_0^3 r_{41}$ by using the system shown in Fig. 4. The source was a tungsten–halogen lamp with interference filters (FWHM = 10 nm) and a spatial filter. A Babinet–Soleil compensator provided the required quarter-wave retardance at each measurement wavelength. The voltage applied to the crystal was sinusoidal. We obtained the quantity $n_0^3 r_{41}$ by determining the modulation depth (the ratio of the signal at frequency ω to the average signal) for a given applied voltage. For these experiments we used a crystal with $h = 1.948 \pm 0.013$ cm, $d = 0.470 \pm 0.013$ cm, and $\delta_S \cong 8°$.

For values of δ_E that are small compared with δ_S, the factor multiplied by δ_E in Eq. (11) becomes $\sin(\delta_S)/\delta_S$. Significant values of residual stress birefringence in the crystal must be taken into account in the measurement of δ_E or r_{41}. However, for the parameters of our experiment, this was not the case. The crystal used in this measurement with $\delta_S \approx 8°$ has a negligible effect on the measurement of r_{41} when compared with the stated uncertainties for our measured values.

We measured the drive voltage with an ac voltmeter. To determine the modulation depth, we used two lock-in amplifiers, one referenced to the voltage applied to the crystal and the other referenced to a chopper. The chopper frequency was approximately 300 Hz and the frequency of the drive voltage was approximately 10 kHz. We measured the modulation depth at several drive voltages and fitted a straight line to the results. Values for crossed and aligned polarizers differed typically by less than 1% and were averaged. We computed $n_0^3 r_{41}$ and r_{41} from these data, knowing the wavelength, the crystal dimensions, and the index of refraction. The results are shown in Table 4, along with previous measurements. All the values in Table 4 were obtained at low frequencies and are therefore constant stress values (sometimes called T values). At frequencies higher than the piezoelectric resonances of the crystal, the values could be higher or lower (constant strain or S values). All our values in Table 4 were obtained at room temperature (23 ± 1 °C).

B. $\mathrm{d}(n_0{}^3 r_{41})/\mathrm{d}Tn_0^3 r_{41}$ Measurements

We obtained data to calculate $\mathrm{d}(n_0^3 r_{41})/\mathrm{d}Tn_0^3 r_{41}$ by using the apparatus shown in Fig. 5. A polarizing beam splitter, such as a Wollaston polarizer, was used as the output polarizer, so that the aligned and crossed polarizer response functions could be obtained simultaneously. The difference over the sum $(R_+ - R_-)/(R_+ + R_-)$ of the two detected signals was taken to obtain a response function that is independent of $\Gamma_{\pm}$ when the two detector gains are well matched. The new response has a functional form of

$$R(\delta_E, \delta_S)_{\Delta/\Sigma} = \delta_E \frac{\sin 2\phi}{2\phi}. \tag{12}$$

Table 4. Electro-Optic Properties of Bismuth Germinate at Low Frequencies

	$n_0^3 r_{41}$ (pm/V)		r_{41} (pm/V)				
λ (nm)	This Study (±0.08)	Ref. 4	This Study (±0.08)	Ref. 3	Ref. 2	Ref. 4 (±0.02)	Ref. 5
305.4		6.2				0.33	
334.5		6.9				0.49	
351.1		7.2				0.57	
363.9		8.4				0.62	
405				0.82 ± 0.02			
440				0.85 ± 0.01			
450					1.03		
457.9		8.5			·	0.85	
488.9		8.5		0.89 ± 0.01	·	0.86	
495					·		
514.5		8.7		0.92 ± 0.01	·	0.89	
542					·		
550	9.97		1.05		·		
600	9.93		1.06		·		
620				0.95 ± 0.01	1.03		
631							
632.8		8.9				0.96	
633	9.86		1.07				1.01
750	9.73		1.08				
800	9.79		1.10				
850	9.86		1.11				
855							1.07
900	9.78		1.11				
950	9.70		1.11				
1000	9.63		1.11				

The normalized temperature dependence of Eq. (12) is

$$\frac{1}{R_{\Delta/\Sigma}}\frac{dR_{\Delta/\Sigma}}{dT} = \left(\frac{1}{n_0^3 r_{41}}\frac{dn_0^3 r_{41}}{dT} + \alpha\right)(1 + K\delta_E^2) + (K\delta_S^2)\frac{1}{\delta_S}\frac{d\delta_S}{dT}, \quad (13)$$

where K is

$$K = \frac{\cot 2\phi}{2\phi} - \frac{1}{4\phi^2}. \quad (14)$$

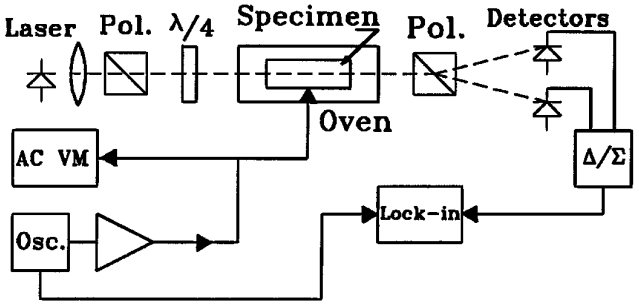

Fig. 5. System for measuring $d(n_0^3 r_{41})/dT$; AC VM, ac voltmeter.

To obtain a value for $d(n_0^3 r_{41})/dT n_0^3 r_{41}$, from the measured signal $R_{\Delta/\Sigma}$, one must evaluate or know the terms of Eq. (13). K has a value of approximately $-\frac{1}{3}$ for $1° < \delta_S < 80°$ and $\delta_E \ll \delta_S$. The term $(1 + K\delta_E^2)$ is nearly equal to 1 for the crystals used in this experiment ($h = 1$ cm, $d = 0.5$ cm, and $\delta_S \sim 2°$), with an applied voltage of approximately 30 V (rms); α is known from earlier measurements. For one of the crystals used, we measured $d\delta_S/dT\delta_S$ to be approximately $(1.1 \pm 0.5) \times 10^{-3}/°\text{C}$, so $(K\delta_S^2)d\delta_S/dT\delta_S = (-4.8 \pm 1.6) \times 10^{-7}/°\text{C}$. With these values, a correction to the measured signal $R_{\Delta/\Sigma}$ can be calculated and $d(n_0^3 r_{41})/dT n_0^3 r_{41}$ is

$$\frac{1}{n_0^3 r_{41}}\frac{dn_0^3 r_{41}}{dT} \approx \frac{1}{R_{\Delta/\Sigma}}\frac{dR_{\Delta/\Sigma}}{dT} - (5.8 \pm 0.5) \times 10^{-6}. \quad (15)$$

The correction term in relation (15) is dominated by the thermal expansion coefficient and is relatively insensitive to our values of $d\delta_S/dT\delta_S$. We assume that this correction term is valid for all of the crystals tested. In general the best measurements are made with δ_S as small as possible, of the order of a few degrees, and with voltages large enough to produce δ_E of a few tens of milliradians.

A typical set of data is shown in Fig. 6. The mean normalized slope for 34 data sets was computed with three different BGO specimens. This yields a $d(n_0^3 r_{41})/dT n_0^3 r_{41}$ value of $(1.54 \pm 0.16) \times 10^{-4}/°\text{C}$, where the uncertainty is reported as one standard deviation. Care was taken that the BGO crystal was not stressed by the electrodes or the mounting fixture. The electrodes were gold, sputtered onto the surface of the crystal. The light source was an approximately 3-nm bandwidth laser diode, to avoid coherence effects, and its central wavelength was 675 nm.

4. Photoelastic Properties

Electro-optic components are subject to uniaxial compressive stress, both directly and as a result of

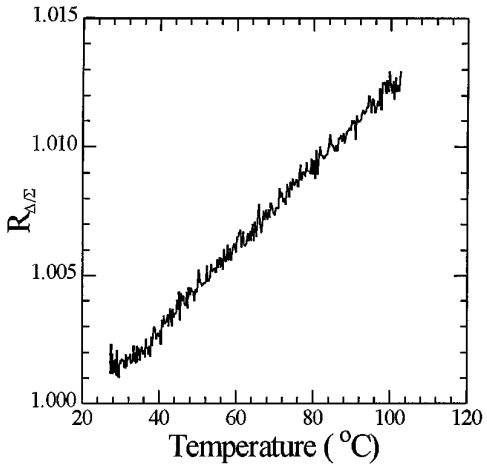

Fig. 6. $R_{\Delta/\Sigma}$ versus temperature in BGO at 670 nm.

temperature inhomogeneities. Stress gives rise to birefringence, which affects the stability of the system. The refractive indices of crystals are related to stress through the stress-optic (sometimes called piezo-optic) tensor, q_{ij}, or to strain through the strain-optic (sometimes called elasto-optic) tensor, p_{ij}. Strain is related to stress through the compliance tensor, s_{ij}, or vice versa through the stiffness tensor, c_{ij}. Each of these is a fourth-rank tensor, commonly represented as a 6×6 matrix. These tensors or matrices describe the photoelastic properties of the crystal. In $\bar{4}3m$ crystals, each tensor has three independent elements, the 11, 12, and 44 matrix elements.[13]

The elements of the compliance and stiffness tensors for BGO have been previously determined at 20 °C by Schweppe.[6] We have measured values $q_{11} - q_{12}$ and q_{44} of the stress-optic tensor directly and, using Schweppe's data, have computed the corresponding strain-optic tensor elements.

A. Stress-Optic Measurements

In a $\bar{4}3m$ crystal, birefringence B induced by a stress applied along the crystallographic (001) direction and observed in the (110) direction is[12–14]

$$B \equiv n_{\parallel} - n_{\perp} = \frac{{n_0}^3}{2}(q_{11} - q_{12})\sigma, \tag{16}$$

where $n_{\parallel}$ and $n_{\perp}$ are the refractive indices for light with its electric vector parallel and perpendicular to the direction of stress, respectively, n_0 is the refractive index of the unstressed crystal, and σ is the applied stress. We use the convention that compressive stresses are positive. Similarly, the birefringence induced by a stress applied along the crystallographic (110) direction and observed in the (001) direction is

$$B \equiv n_{\parallel} - n_{\perp} = \frac{{n_0}^3}{2} q_{44}\sigma. \tag{17}$$

Using specimens oriented as shown in Fig. 7, we are thus able to determine both $q_{11} - q_{12}$ and q_{44} on the same specimen.

We determined the stress-induced birefringence by measuring the stress-induced retardance. The measured retardance is related to the induced birefringence by

$$\delta_{\sigma} = \frac{2\pi}{\lambda}(n_{\parallel} - n_{\perp})h, \tag{18}$$

where λ is the vacuum wavelength and h is the propagation path length through the crystal.

The stressing apparatus used is the same as that in Ref. 14 and can apply stresses up to approximately 10^8 N/m^2 on our crystals. The induced retardance was measured polarimetrically for each stress by determination of the ellipticity of the emerging light when the input light was linearly polarized at 45° to the direction of applied stress. A Babinet–Soleil compensator was used to determine the sign of the induced retardance. These measurements were made at approximately 23 °C.

Figure 8 shows a sample of the data obtained by this method for the stress along the (110) direction. In some cases, the samples tested exhibited a small amount (<10°) of birefringence in the absence of applied stress. The stress-optic tensor elements were therefore computed from the slope of the best-fit straight line of retardance versus stress, rather than absolute retardance at a given stress, and birefringence data at zero stress was not used in the slope calculation. The necessary index of refraction values were those reported above. The values of the stress-optic coefficients are given in Table 5. Each measured coefficient represents the average of six measurements on three different specimens. The total uncertainty is reported as the standard deviation of the mean of the six measurements.

B. Strain-Optic Tensor Elements

For $\bar{4}3m$ crystals, the strain-optic tensor elements are related to the stress-optic tensor elements by the relations[15,16]

$$p_{44} = q_{44}c_{44}, \tag{19}$$

$$p_{11} - p_{12} = (q_{11} - q_{12})(c_{11} - c_{12}). \tag{20}$$

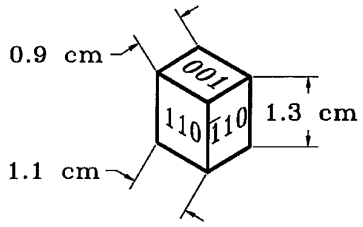

Fig. 7. Geometry of specimens used for the stress-optic measurements.

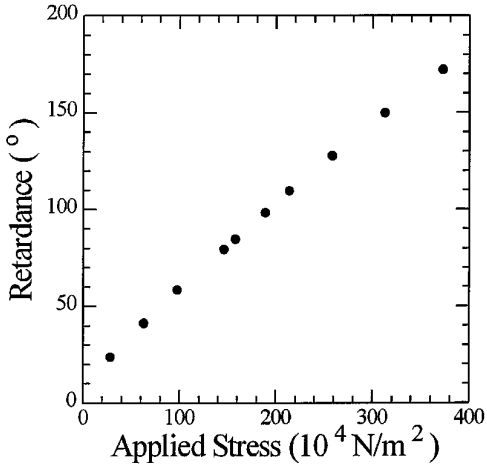

Fig. 8. Typical data for the determination of q_{44}.

Table 5. Photoelastic Constants of Bismuth Germanate at a Wavelength of 632.8 nm

$n_0^3(q_{11} - q_{12})$	$(-2.764 \pm 0.143) \times 10^{-12}\ \mathrm{m^2/N}$	This study
$n_0^3 q_{44}$	$(-1.260 \pm 0.130) \times 10^{-11}\ \mathrm{m^2/N}$	
$q_{11} - q_{12}$	$(-2.995 \pm 0.155) \times 10^{-13}\ \mathrm{m^2/N}$	This study and Ref. 3
q_{44}	$(-1.365 \pm 0.141) \times 10^{-12}\ \mathrm{m^2/N}$	
c_{11}	$1.158 \times 10^{11}\ (\pm 1\%)\ \mathrm{N/m^2}$	Ref. 6
c_{12}	$0.270 \times 10^{11}\ (\pm 8\%)\ \mathrm{N/m^2}$	
c_{44}	$0.436 \times 10^{11}\ (\pm 1\%)\ \mathrm{N/m^2}$	
$p_{11} - p_{12}$	-0.0266 ± 0.0023	This study and Ref. 6
p_{44}	-0.0595 ± 0.0068	
$n_0^3(p_{11} - p_{12})$	-0.245 ± 0.021	This study and Ref. 6
$n_0^3 p_{44}$	-0.549 ± 0.063	

Using Schweppe's data[6] for the stiffness tensor elements, we obtain the values given in Table 5. The uncertainties are the sum of the magnitudes of the uncertainties in the stress-optic and stiffness tensor elements.

5. Conclusions

The data reported here affirm that bismuth germanate is a suitable material for those applications of the electro-optic effect in which precision is more important than sensitivity. Though the electro-optic effect is not large, it is relatively stable with temperature. The stress-optic effect is not substantially larger than for other materials that might be considered. Thus, the stability of sensors using BGO is limited by the small temperature dependence of the electro-optic effect and not by the large temperature-dependent natural crystalline birefringence found in other electro-optic crystals.

Appendix A.

To model a BGO crystal with linear stress birefringence, we use Jones calculus.[17] The resulting field for a beam of linearly polarized light passing through a quarter-wave plate at 45°, an electro-optic crystal with stress induced birefringence, and a polarizer is

$$\begin{bmatrix} E_x \\ E_y \end{bmatrix} = \begin{bmatrix} 1 & 0 \\ 0 & 0 \end{bmatrix} \begin{bmatrix} A & B \\ C & D \end{bmatrix} \frac{1}{\sqrt{2}} \begin{bmatrix} 1 & i \\ i & 1 \end{bmatrix} \begin{bmatrix} E_x \\ 0 \end{bmatrix}, \tag{A1}$$

where $\mathbf{E}$ is the electric field vector of the light, and A, B, C, and D are the Jones matrix components that describe the electro-optic crystal. The Jones matrix for the electro-optic crystal with stress-induced birefringence has been developed by Lee.[18] That matrix is used here, with the correction of a few typographical errors and the assumptions that there is no Faraday rotation in the crystal and that δ_E and δ_S are both much smaller than 1 rad. The Jones matrix components are then

$$A = \cos\phi - i\delta_S \frac{\sin\phi}{2\phi} = D^*,$$

$$B = \frac{1}{2} i\delta_E \frac{\sin\phi}{\phi} = C, \tag{A2}$$

where

$$\phi \cong \frac{1}{2}(\delta_S^2 + \delta_E^2)^{1/2}, \tag{A3}$$

and where δ_S is the stress birefringence and δ_E is the electro-optic retardance proportional to applied voltage V. Equations (A2) and (A3) were developed with the assumption that the axes of δ_S are 45° with respect to the axes of δ_E. The intensity response of a BGO crystal with stress birefringence using Eqs. (A1), (A2), and (A3) is

$$R(\delta_E, \delta_S)_\pm = \Gamma_\pm \left(1 \pm \delta_E \frac{\sin 2\phi}{2\phi}\right), \tag{A4}$$

where $\Gamma_\pm$ is equal to $\frac{1}{2}\gamma_\pm |E_x|^2$ and where $\gamma_\pm$ is a constant dependent on the optical coupling. The $\pm$ in Eq. (A4) refers to the orientation of the output polarizer in Eq. (A1). The + represents an output polarizer crossed with the input polarization state, and the − represents an output polarizer aligned with the input polarization state.

This research was supported in part by the Bonneville Power Administration, the Electric Power Research Institute, and the Empire State Electric Energy Research Corporation through the Bonneville Power Administration, the Los Alamos National Laboratory, the Department of the Navy through the Naval Surface Warfare Center Carderock Division, and NASA Lewis Research Center.

References

1. S. Weikel and G. Stranovshky, "Application of an electro-optic voltage transducer at 345 kV," in *Proceedings of the EPRI Workshop on Optical Sensors for Utility T&D Applications* (Electric Power Research Institute, Palo Alto, Calif., 1996); K. Kurosawa, "Development and field tests of optical fiber sensors for electric power systems," in *Proceedings, 7th International Conference on Optical Fiber Sensors* (Institution of Radio and Electronics Engineers Australia, Edgecliff, NSW, 1990), pp. 67–72; G. W. Day, P. D. Hale, M. N. Deeter, T. E. Milner, D. Conrad, and S. M. Etzel, "Limits to the precision of electro-optic and magneto-optic sensors," Natl. Bur. Stand. (U.S.) Tech. Note **1307,** 3-1–4-23 (1987); M. Kanoi, G. Takahashi, T. Sato, M. Higaki, E. Mori, and K. Okamura, "Optical voltage and current measuring system for electric power

systems," IEEE Trans. Power Deliv. **PWRD-1,** 91–97 (1986); B. N. Nelson, C. Menzel, and T. G. DiGiuseppe, "Fiber-optic electric field sensor configurations for high bandwidth lightning research measurement applications," in *High Bandwidth Analog Applications of Photonics,* J. S. Chang, ed., Proc. SPIE **720,** 85–90 (1986); K. Shibata, "A fibre optic electric field sensor using the electro-optic effect of $Bi_4Ge_3O_{12}$," in *Proceedings, First International Conference on Optical Fibre Sensors* (Institution of Electrical Engineers, London, 1983), pp. 164–168.

2. R. Nitsche, "Crystal growth and electro-optic effect of bismuth germanate, $Bi_4(GeO_4)_3$," J. Appl. Phys. **36,** 2358–2360 (1965).
3. D. P. Bortfeld and H. Meier, "Refractive indices and electro-optic coefficients of the eulytites $Bi_4Ge_3O_{12}$," J. Appl. Phys. **43,** 5110–5111 (1972).
4. G. Montemezzani, S. Pfändler, and P. Günter, "Electro-optic and photo refractive properties of $Bi_4Ge_3O_{12}$ crystals in the ultraviolet spectral range," J. Opt. Soc. Am. B **9,** 1110–1117 (1992).
5. O. Kamada and K. Kakishita, "Electro-optical effect of $Bi_4Ge_3O_{12}$ crystals for optical voltage sensors," Jpn. J. Appl. Phys. **32,** 4288–4291 (1993).
6. H. Schweppe, "Electro-mechanical properties of bismuth germanate, $Bi_4(GeO_4)_3$," IEEE Trans. Sonics Ultrason. **SU-16,** 219 (1969).
7. R. S. Longhurst, *Geometrical and Physical Optics* (Longmans, London, 1973), Chap. 5, pp. 82–89.
8. M. Young, "Refracted ray scanning," Natl. Bur. Stand. (U.S.) Spec. Publ. **637,** 130–134 (1982).
9. A. Feldman, D. Horowitz, R. M. Waxler, and M. J. Dodge, "Optical materials characterization," Natl. Bur. Stand. (U.S.) Tech. Note **993,** 7–15 (1979).
10. H. Barrel and J. E. Sears, "The refraction and dispersion of air for the visible spectrum," Philos. Trans. R. Soc. London **238,** 1–64 (1940).
11. M. Born and E. Wolf, *Principles of Optics,* 6th ed. (Pergamon, New York, 1980), Chap. 7, p. 330.
12. S. Namba, "Electro-optic effect in zincblende," J. Opt. Soc. Am. **51,** 76–79 (1961).
13. A. Yariv and P. Yeh, *Optical Waves in Crystals* (Wiley, New York, 1984), Chap. 7, pp. 220–275.
14. A. Feldman and W. J. McKean, "Improved stressing apparatus for photoelasticity measurements," Rev. Sci. Instrum. **46,** 1588–1589 (1975).
15. T. S. Narasimhamurty, *Photoelastic and Electro-Optic Properties of Crystals* (Plenum, New York, 1981), Chap. 2, pp. 23–45; Chap. 5, pp. 197–274.
16. J. F. Nye, *Physical Properties of Crystals* (Oxford, U. Press, New York, 1964), Chap. 1, pp. 3–32.
17. R. C. Jones, "A new calculus for the treatment of optical systems," J. Opt. Soc. Am. **31,** 488–493 (1941); W. A. Shurcliff, *Polarized Light* (Harvard U. Press, Cambridge, Mass., 1962), Chap. 8, pp. 107–123.
18. K. S. Lee, "New compensation method for bulk optical sensors with multiple birefringences," Appl. Opt. **28,** 2001–2011 (1989).